Journal of Physics D: Applied Physics

**PAPER**

# Streamer propagation characteristics of nanosecond pulsed discharge plasma on fluidized particles surface: experimental investigation and numerical simulation

To cite this article: Ju Li *et al* 2024 *J. Phys. D: Appl. Phys.* **57** 255203

IOP Publishing
Journal of Physics D: Applied Physics
J. Phys. D: Appl. Phys. **57** (2024) 255203 (14pp)
https://doi.org/10.1088/1361-6463/ad33f8

# Streamer propagation characteristics of nanosecond pulsed discharge plasma on fluidized particles surface: experimental investigation and numerical simulation

**Ju Li[1], Nan Jiang[1,*], Xiaolong Wang[3], Guanglin Yu[1], Bangfa Peng[2], Junwen He[1] and Jie Li[1,*]**

[1] School of Electrical Engineering, Dalian University of Technology, Dalian 116024, People's Republic of China
[2] Shanxi Key Laboratory of Mining Electrical Equipment and Intelligent Control, School of Electrical and Power Engineering, Taiyuan University of Technology, Taiyuan 030024, People's Republic of China
[3] School of Electrical Engineering, Shandong University, Jinan 250061, People's Republic of China

E-mail: jiangnan@dlut.edu.cn and lijie@dlut.edu.cn

Received 14 October 2023, revised 11 February 2024
Accepted for publication 14 March 2024
Published 26 March 2024

**Abstract**

Plasma fluidized-bed contributes to strengthening the interaction between active species in plasma and fluidized powder particles, resulting in higher active species utilization efficiency and superior powders processing/modification performance. However, the plasma streamer dynamics on the fluidized powder particles are still unclear due to the intricacy of plasma fluidized-bed. In this work, the time-resolved evolution behavior of plasma streamers on fluidized powder particles surfaces has been explored in plasma fluidized-bed system based on a simplified pin-cylinder configuration. The results reveal that the entire streamer propagation process includes volume discharge and surface discharge. The maximum electron density generated by surface discharge is one order of magnitude higher than that produced by volume discharge, indicating that surface discharge plays a dominant role in powder particles modification. The presence of fluidized particle will cause streamer branching, and the main streamer splits into two independent sub-streamers for propagation in a 'parabola-like' shape. Compared with large-size fluidized particles (1000 $\mu$m), streamer wraps a larger area on micron-size fluidized particles (200 $\mu$m), with a 78% increase in the coverage area, which is favorable to the modification of powder particles. Furthermore, the evolution of active species on fluidized particle surface is analyzed. The active species (N, O, $O_2^-$) are mainly distributed around the north pole, and $N_2^+$ is mainly distributed between 25° and 50° of the particles. With the decrease of fluidized particle size, the polarization effect between particles is significantly enhanced, and the maxima of the number densities of active species increase. These findings help to get a better understanding of the interaction between plasma and fluidized particles in fluidized systems.

* Authors to whom any correspondence should be addressed.

Keywords: nanosecond pulsed discharge, plasma fluidized-bed system, streamer propagation, plasma modification, reactive species number densities

## 1. Introduction

Atmospheric pressure low-temperature plasma is enriched with a variety of reactive species, including energetic electrons, ions, excited atoms or molecules and free radicals. Due to its advantages of environmental friendliness, simple operation, shorter processing time and energy conservation [1–3], plasma has been widely applied in the field of material modification, such as the surface functionalization of polymers [4, 5]. Plasma can jointly change adhesion of polymer surface through one or several mechanisms e.g. surface cleaning, etching, chain scission and crosslinking as well as chemical modification. The reactive species play a dominant role in the plasma modification process. It has been reported that plasma modification is mainly due to the interaction between reactive species and polymer surfaces [6–8]. The reactive species can impact the material surface, and physical or chemical reactions occur. After plasma treatment, some surface properties will be improved, like surface roughness, free energy and hydrophilicity and hydrophobicity. However, despite these advancements, there are still some critical issues in the treatment of powder materials, which limit its extensive application. One of the challenges is how to achieve a homogenous, uniform and efficient material treatment method.

As a powder batch processing technology with mature industrial system, plasma fluidized-bed system can enhance flow mixing between gas and particles, high mass transfer rates, and enable uniform powder processing [9]. A gas fluidized-bed is established by passing gas upward through a fixed-bed of particles [10]. As the gas velocity reaches the critical fluidization velocity, the pressure drop counterbalances the weight of solid particles, which will cause the particles to be suspended in the upward-flowing gas. Fluidized particles have a broad particle-size distribution, spanning from a few micrometers to several millimeters. Since the possibility of combining plasma and fluidized-bed system was reported by Derco in 1984 [11], there have been some attempts to employ plasma fluidized-bed for particle processing and preparation. Chen *et al* [12] designed an atmospheric pressure He plasma fluidized-bed to modify calcium carbonate powders in the hexamethyldisiloxane. The results showed that the surface properties changed from super-hydrophilicity to super-hydrophobicity. Yao *et al* [9] synthesized uniform, low-temperature $TiO_2$@C nanocomposite by fluidized-bed plasma-enhanced chemical vapor deposition with a mixture of $CH_4$ and Ar. Soto *et al* [13] prepared $Ag/SiO_2$ nanocomposite in an Ar fluidized-bed microwave plasma reactor and the result demonstrated that the nanocomposite had obvious bactericidal effect on *Escherichia coli*. Bouchoul *et al* [14] compared the plasma-catalysis coupling of $CH_4$ and $CO_2$ conversion in plasma fixed-bed and fluidized-bed systems. The results showed that the conversion was higher in the fluidized-bed system, indicating that the interaction between catalyst particles and plasma is enhanced. Dasan *et al* [15] studied the inactivation efficiency for aflatoxigenic spores of *Aspergillus flavus* and *Aspergillus parasiticus* on hazelnuts in air or $N_2$ fluidized-bed plasma system. The results showed that the air plasma system was more effective than nitrogen plasma system. In our previous work, a DBD plasma fluidized-bed system was designed and employed to remediate atrazine-contaminated soil, realizing efficient remediation of contaminated soil [16].

The present work predominantly focuses on the application and treatment of plasma fluidized-bed. Nevertheless, to the best of our knowledge, there are almost no literature focus on exploring the plasma streamer propagation in plasma fluidized-bed, which is crucial to reveal the underlying mechanism of plasma-particles interaction. On the one hand, the discharge within a plasma fluidized-bed is a highly dynamic process that may involve time scales ranging from nanoseconds to minutes. Therefore, it is challenging to obtain high-resolution spatio-temporal data and perform accurate analysis. On the other hand, the interactions between plasma and particles in the fluidized-bed encompass physical processes at different scales, from microscopic plasma phenomena to macroscopic fluid flow. Plasma numerical simulation, as a competitive computer modeling tool, can simulate the streamer propagation mechanism inside the reactor and provide important insights for in-depth understanding of plasma discharge characteristics. So far, however, almost all previous literature on plasma experiments and numerical simulation are fixed-bed systems [17–29].

To gain a deeper understanding of the discharge characteristics in the plasma fluidized-bed, it is necessary to construct a complex model that encompasses a variety of physical processes and interactions. However, due to the intricacy of system, it is often necessary to simplify experimental setups and numerical models. Firstly, it is assumed that the particles remain stationary during this process because the formation and propagation process of plasma is fast (nanoseconds). Secondly, the shape of the particles is set to a regular spherical structure. Finally, it is assumed that the spacing between particles remains constant. Based on this, in this work, a time-resolved intensified charge-coupled device (ICCD) camera is used to capture the fluidization evolution behavior of plasma on the particle surface in a fluidized-bed system. Polytetrafluoroethylene rod ($\varepsilon = 2.1$) with a diameter of 1000 $\mu$m is used to simulate the fluidized particles. Furthermore, the discharge behavior between the plasma and fluidized particles is studied based on a two-dimensional (2D) fluid model, which is used to explain the experimental results. The outline of this paper is as follows. The experiment

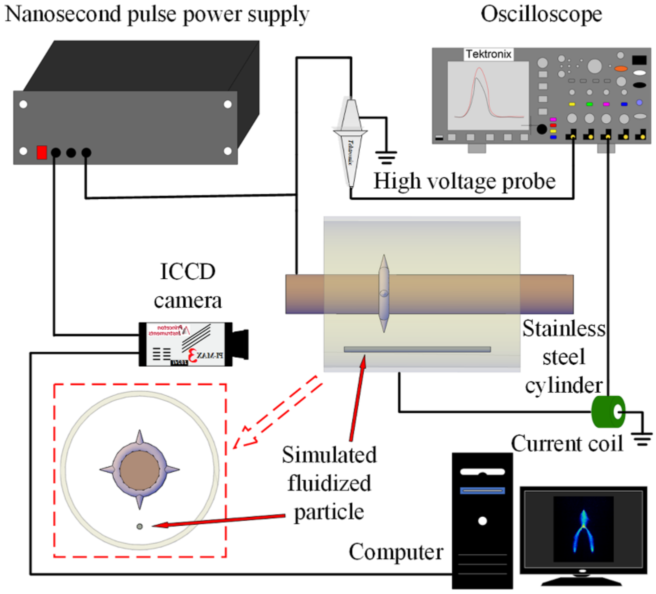


**Figure 1.** The experimental system diagram for time-resolved discharge device.

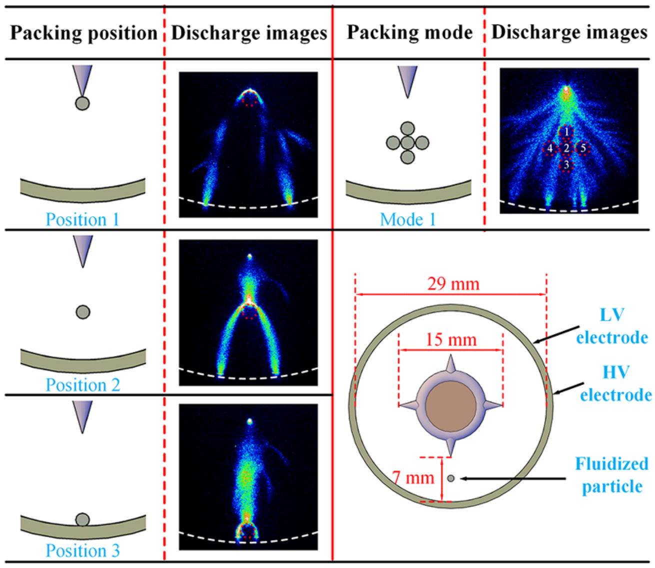


**Figure 2.** Packing position and packing mode of the fluidized particles and discharge images.

conditions and simulation model are introduced in sections 2. In section 3, the obtained experimental and numerical simulation results will be analyzed and discussed. At the same time, the streamer propagation characteristics of plasma with micron-size particle size (200 $\mu$m) in fluidization system are simulated by the model. Finally, conclusion is drawn in section 4.

## 2. Experiment and model

### 2.1. Experimental setup

A schematic diagram of the experimental apparatus is presented in figure 1, which mainly includes the following components: nanosecond pulsed power supply, reaction system, electrical measurement system and ICCD camera. The pulse power supply (HVP-20P) is developed by Xi'an Smart Maple Electronic Technology Co. Ltd. A voltage amplitude is set at 14 kV. Both the rising and falling time are 50 ns. The voltage and current generated during the discharge process are measured by a high-voltage probe (Tektronix P6015A) and a current coil (Pearson 6595), displayed on a digital oscilloscope (Tektronix DPO3012 100 MHz). The acquisition frequency of oscilloscope is 2.5 GHz s$^{-1}$. In order to explore the time-resolved evolution of plasma streamer propagation process, the ICCD camera (Princeton, PI-MAX 3 1024i) is used to capture the time-resolved images, and the exposure time is set as 3 ns and 5 ns. The images in the experiment are obtained under different single pulse discharge conditions. The ICCD camera is triggered by an external pulse power source and maintains synchronization with the high-voltage pulse.

In order to observe the streamer evolution more clearly, the simplified plasma fluidized-bed system configuration is composed of a multi-pin high voltage electrode and a stainless steel cylinder low voltage electrode. The linear distance between the two pin tips of the high-voltage electrode is 15 mm, and the inner diameter, wall thickness and length of the cylinder are 29 mm, 1 mm, and 150 mm, respectively. The distance from the pin tip to the cylinder is 7 mm, and the radius of curvature is approximately 40 $\mu$m. The cross-section of the polytetrafluoroethylene rod is used to simulate the size of the fluidized particles. The diameter of the fluidized particles is 1000 $\mu$m. The specific spatial arrangements of the fluidized particles and the corresponding discharge images are shown in figure 2. The fluidized particles are placed at different positions between high-voltage pin electrode and the cylindrical ground electrode to better conform to the randomness of particle motion in the fluidized-bed. The fluidized particles are placed at the pin tip, 3.5 mm away from the pin tip and the surface of the cylinder, which are defined as positions 1, 2 and 3 respectively. In a real fluidization system, since the fluidized particles are in a fluidization state, there will be a certain distance between fluidized particles during fluidization. Therefore, two distances of fluidized particles are studied, and the distances between adjacent fluidized particles are set to 0.1 mm and 0.5 mm, respectively. The gap size is much larger than the Debye length 0.52 $\mu$m. In mode 1, five fluidized particles are arranged in the form of crosses. In the above mode, the fluidized particles are assigned distinct numbers.

### 2.2. Simulation model description

PASSKEy (PArallel Streamer Solver with KinEtics) code is used for modeling to study streamer propagation. At present, the numerical simulation code has been applied to the modeling of surface streamer discharge [30–33], the packed-bed discharge [34] and the effect of the rotating dielectric plate on streamer channel [35]. In this work, the PASSKEy code

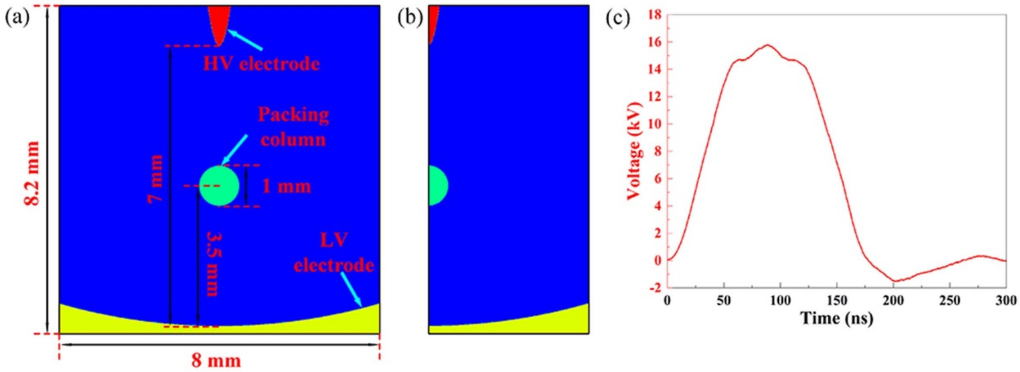


**Figure 3.** (a) The geometry of the numerical model; (b) computational domain of the axisymmetric model; (c) applied voltage in the simulation.

proposed by Zhu *et al* has been validated with a benchmark case of streamer propagation for a point-to-plate configuration [36–38]. In principle, streamer propagation on the surface of fluidized particle should be studied in three dimensions (3D) to conform to the particle geometry in experimental fluidized-bed reactor. However, modeling with 3D geometry will lead to a significant increase in calculation time. Hence, a smart approximation is used for the 3D geometry without compromising its authenticity. In order to save computation time, a two-dimensional (2D) axisymmetric fluid model is constructed to model the pin-to-cylinder configuration. The simulation model employs a cross-sectional geometry of the pin-to-cylinder configuration that resembles the structure of the top view of the pin-to-cylinder configuration, and the size of the numerical simulation model is consistent with that of the experimental device. The dimensions of the simulation geometry are shown in figure 3. It is worth noting that the 2D approximation would actually exhibit a torus-shape after rotation, which is different from the reality. However, this model primarily focuses on the plasma behavior on the surface of fluidized particle, and the model provides a qualitative description of the discharge, which is not affected by this torus shape. In addition, the same smart approximation has been reported in the literatures [25, 26]. The streamer propagation exhibits a same process at each pin electrode, so the streamer propagation characteristics of a single pin electrode are simulated. The pin boundary is confined by implementing a parabola curve with a curvature radius of 40 $\mu$m along the central cross-section of the pin electrode. The size of mesh cells near the pin electrode region and fluidized particle is set as 4 $\mu$m, and the total number of nodes in the computational domain is 750 395. The voltage waveform is shown in figure 3(c).

All experiments are conducted at room temperature and atmospheric pressure. In the simulation, the volume fraction of $N_2$ and $O_2$ is set as 0.8 and 0.2, and the temperature and pressure are kept constant at 300 K and 1 atm respectively. Atmospheric pressure air plasma involves dozens of species and potentially hundreds of complex reactions, including electron collision, excitation, and ionization, as well as quenching of excited species, charge exchange and electron-ion recombination reactions, which makes it challenging to incorporate all these species and reactions into the plasma modeling process. To address this complexity, simplified reaction sets are adopted. Some surface reactions involving the complex chemistry at fluidized particle surface is not accounted for in the model, and the chemistry reactions happen only in the volume discharge. The simulation model contains 17 plasma active species, including electron, neutral atoms, ions and excited species, and 40 gas phase reactions between the above species. Among them, singlet oxygen, as the lowest excited state of $O_2$, is also an important reactive oxygen species [39, 40]. However, there is report indicating that collisions with $O_3$ can quench singlet oxygen, which makes it a minor species in most gas mixtures [41]. Since this model does not consider the reactions about $O_3$ species, the singlet oxygen is not accounted for. The insights obtained in this study may provide guidance for future research of more complex molecular gases. The specific plasma reaction set is given in the table 1. Figure 4 shows the rate coefficients of the electron-impact processes (R1)–(R8), as functions of the mean electron energy, which is obtained from the Boltzmann solutions. Furthermore, Poisson equation for electric field, drift-diffusion equations for species, electron energy conservation equation and Helmholtz equations for photoionization are solved via the plasma model. All of the equations and mathematical methods could be found in paper [32, 33, 37, 38]. The equations solved in the simulation process are briefly introduce as follows:

The electric potential is obtained from the solution of Poisson's equation:

$$\nabla\left(\varepsilon_0\varepsilon_r\nabla\Phi\right) = -\sum_{i=1}^{N_{\mathrm{ch}}} q_i n_i - \rho_c. \quad (1)$$

**Table 1.** Plasma reaction set with rate coefficients used in this model. ($T_e$ is the electron temperature (eV) and $T_g$ represents the gas temperature (K)).

| No. | Reaction | Rate coefficient | References |
|---|---|---|---|
| R1 | $e + N_2 \rightarrow 2e + N_2^+$ | Figure 4 | [44] |
| R2 | $e + O_2 \rightarrow 2e + O_2^+$ | Figure 4 | [45] |
| R3 | $e + O_2 \rightarrow O + O^-$ | Figure 4 | [45] |
| R4 | $e + N_2 \rightarrow e + N_2(A^3\sum)$ | Figure 4 | [44] |
| R5 | $e + N_2 \rightarrow e + N_2(B^3\Pi)$ | Figure 4 | [44] |
| R6 | $e + N_2 \rightarrow e + N_2(C^3\Pi)$ | Figure 4 | [44] |
| R7 | $e + O_2 \rightarrow e + O + O$ | Figure 4 | [46] |
| R8 | $e + O_2 \rightarrow e + O + O(^1D)$ | Figure 4 | [46] |
| R9 | $e + O_4^+ \rightarrow O + O + O_2$ | $1.4 \times 10^{-6} \times (300/T_e)^{0.5}$ | [47] |
| R10 | $e + O_2^+ \rightarrow O + O$ | $2 \times 10^{-7} \times (300/T_e)$ | [48] |
| R11 | $e + O_2 + O_2 \rightarrow O- 2 + O_2$ | $1.4 \times 10^{-29} \times (300/T_e) \times \exp(-600/T_g)$ $\times \exp((700 \times (T_e - T_g))/(T_e \times T_g))$ | [48] |
| R12 | $e + N_4^+ \rightarrow N_2 + N_2(C^3\Pi)$ | $2 \times 10^{-6} \times (300/T_e)^{0.5}$ | [49] |
| R13 | $e + N_2^+ \rightarrow N + N$ | $2 \times 10^{-7}$ | [50] |
| R14 | $N_2^+ + N_2 + N_2 \rightarrow N_4^+ + N_2$ | $5 \times 10^{-29}$ | [48] |
| R15 | $N_2^+ + N_2 + O_2 \rightarrow N_4^+ + O_2$ | $5 \times 10^{-29}$ | [51] |
| R16 | $N_4^+ + O_2 \rightarrow O_2^+ + N_2 + N_2$ | $2.5 \times 10^{-10}$ | [48] |
| R17 | $N_2^+ + O_2 \rightarrow O_2^+ + N_2$ | $6.0 \times 10^{-11}$ | [52] |
| R18 | $O_2^+ + N_2 + N_2 \rightarrow O_2^+{\cdot}N_2 + N_2$ | $9.0 \times 10^{-31}$ | [47] |
| R19 | $O_2^+{\cdot}N_2 + N_2 \rightarrow O_2^+ + N_2 + N_2$ | $4.3 \times 10^{-10}$ | [47] |
| R20 | $O_2^+{\cdot}N_2 + O_2 \rightarrow O_4^+ + N_2$ | $1.0 \times 10^{-9}$ | [47] |
| R21 | $O_2^+ + O_2 + N_2 \rightarrow O_4^+ + N_2$ | $2.4 \times 10^{-30}$ | [47] |
| R22 | $O_2^+ + O_2 + O_2 \rightarrow O_4^+ + O_2$ | $2.4 \times 10^{-30} \times (300/T_g)^{3.2}$ | [48] |
| R23 | $O_2^- + O_4^+ \rightarrow O_2 + O_2 + O_2$ | $1.0 \times 10^{-7}$ | [47] |
| R24 | $O_2^- + O_4^+ + N_2 \rightarrow O_2 + O_2 + O_2 + N_2$ | $2.0 \times 10^{-25}$ | [47] |
| R25 | $O_2^- + O_4^+ + O_2 \rightarrow O_2 + O_2 + O_2 + O_2$ | $2.0 \times 10^{-25}$ | [47] |
| R26 | $O_2^- + O_2^+ + N_2 \rightarrow O_2 + O_2 + N_2$ | $2 \times 10^{-25} \times (300/T_g)^{2.5}$ | [48] |
| R27 | $O_2^- + O_2^+ + O_2 \rightarrow O_2 + O_2 + N_2$ | $2 \times 10^{-25} \times (300/T_g)^{2.5}$ | [48] |
| R28 | $O^- + N_2^+ \rightarrow O + N + N$ | $1.0 \times 10^{-7}$ | [48] |
| R29 | $N_2(C^3\Pi) \rightarrow N_2(B^3\Pi)$ | $2.45 \times 10^{7}$ | [47] |
| R30 | $N_2(C^3\Pi) + N_2 \rightarrow N_2(B^3\Pi) + N_2$ | $1.0 \times 10^{-11}$ | [52] |
| R31 | $N_2(C^3\Pi) + O_2 \rightarrow N_2 + O + O(^1D)$ | $3.0 \times 10^{-10}$ | [52] |
| R32 | $N^+ + O_2 \rightarrow N + O_2^+$ | $2.8 \times 10^{-10}$ | [48] |
| R33 | $O^+ + O_2 \rightarrow O_2^+ + O$ | $2.1 \times 10^{-11}$ | [53] |
| R34 | $O^- + O \rightarrow e + O_2$ | $1.4 \times 10^{-10}$ | [47] |
| R35 | $O_2^- + O \rightarrow e + O + O_2$ | $1.0 \times 10^{-10}$ | [54] |
| R36 | $N_2(A^3\sum) + O_2 \rightarrow N_2 + O + O$ | $2.54 \times 10^{-12}$ | [48] |
| R37 | $N_2(B^3\Pi) + O_2 \rightarrow N_2 + O + O$ | $3 \times 10^{-10}$ | [48] |
| R38 | $N_2(B^3\Pi) + N_2 \rightarrow N_2(A^3\sum) + N_2$ | $5.0 \times 10^{-11}$ | [48] |
| R39 | $O(^1D) + O_2 \rightarrow O + O_2$ | $4.0 \times 10^{-11}$ | [52] |
| R40 | $O(^1D) + N_2 \rightarrow O + N_2$ | $2.6 \times 10^{-11}$ | [52] |

$$\frac{\partial \rho_c}{\partial t} = \sum_{j=1}^{N_{ch}} q_j \left[-\nabla \cdot \Gamma_j\right]. \quad (2)$$

where $n_i$,$q_i$, and $\Gamma_i$ are the number density, charge, and flux of each species $i$, respectively. $\Phi$ is the electric potential. $\varepsilon_0$ is the permittivity of vacuum space, $\varepsilon_r$ denotes the relative permittivity of the dielectric ($\varepsilon_r = 2.1$ in this work), and $\rho_c$ represents the surface charge density satisfying the continuity equation for charges on surfaces. $N_{ch}$ is the numbers of charged species.

The drift-diffusion-reaction equations for species are:

$$\frac{\partial n_i}{\partial t} + \nabla \cdot \Gamma_{\mathbf{i}} = S_i + S_{ph}, i = 1, 2, \ldots, N_{total}. \quad (3)$$

$$\Gamma_i = -D_i \nabla n_i - \left(\frac{q_i}{|q_i|}\right) \mu_i n_i \nabla \Phi, i = 1, 2, \ldots, N_{charge}. \quad (4)$$

where $S_i$ denote source function for species $i$. The source function $S_i$ includes production and loss terms due to gas phase reactions and is calculated with detailed kinetics, and $S_{ph}$ is the photoionization source term for electrons and oxygen ions and can be calculated by three-term Helmholtz equations [42, 43]. $D_i$ and $\mu_i$ are the diffusion coefficients and mobility of charged species, the electron swarm parameters and the rate coefficients of electron impact reactions are represented as explicit functions of the reduced electric field *E/N* based on local

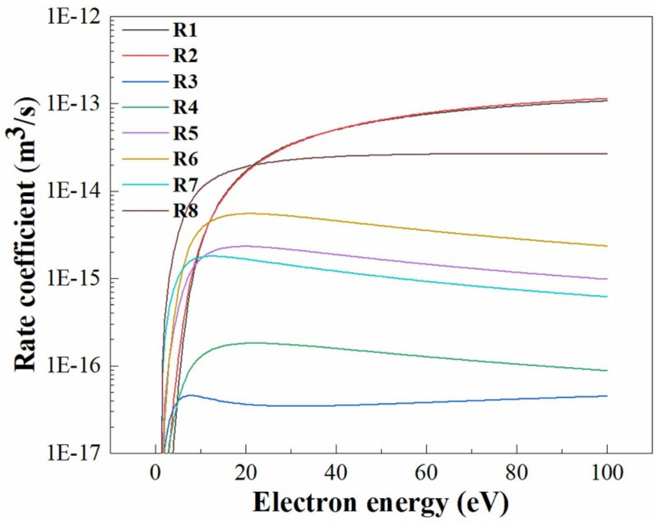


**Figure 4.** The rate coefficients of electron-$N_2$ and electron-$O_2$ determined from zero-dimensional solution of Boltzmann equation.

mean energy approximation. $N_{\text{total}}$ and $N_{\text{charge}}$ represent the number of all species and charged species in kinetics scheme, respectively.

The electron energy equation for mean electron energy is as follows:

$$\frac{\partial}{\partial t}\left(n_{\mathrm{e}}\epsilon_{\mathrm{m}}\right)+\nabla\cdot\Gamma_{\epsilon}=-\left|q_{\mathrm{e}}\right|\cdot\Gamma_{\mathrm{e}}\cdot E-P\left(\epsilon_{\mathrm{m}}\right). \tag{5}$$

$$\Gamma_{\epsilon}=-n_{\mathrm{e}}\epsilon_{\mathrm{m}}\mu_{\epsilon}E-D_{\epsilon}\nabla\left(n_{\mathrm{e}}\epsilon_{\mathrm{m}}\right). \tag{6}$$

$$E=-\nabla\Phi. \tag{7}$$

where is $\epsilon_{\mathrm{m}}$ the mean electron energy and $\boldsymbol{E}$ represents the electric field. $P\left(\epsilon_{\mathrm{m}}\right)$ represents the power lost by electrons in collisions. $\Gamma_{\epsilon}$, $\mu_{\epsilon}$ and $D_{\epsilon}$ are the flux, mobility and diffusivity coefficient of electron energy, respectively.

## 3. Results and discussion

### 3.1. Time-resolved evolution without and with single fluidized particle

Figure 5(a) shows spatiotemporal evolution images of streamer discharge without fluidized particle captured by an ICCD camera with a gate width of 3 ns, and the applied voltage is 14 kV. It should be noted that the above evolution process is obtained in several different main streamers and ordered in temporal sequence. It can be seen from the figure that the streamer discharge starts at 33 ns, and the main streamer propagates from the anode pin electrode to the cathode curved surface. At around 45 ns, the streamer head reached the cathode surface. In general, there will be streamer branching phenomenon when the positive main streamers propagate from the anode pin electrode [55–57]. As shown in the figure 5(a), before the streamer reaches the center of the discharge gap (39 ns), the main streamer propagates in a non-branching state. The spatial distributions of the light emission in the direction of propagation is almost uniform. After that (42 ns), several streamer branches appear outside the main streamer channel. Furthermore, clear streamer branches can be seen from the last long exposure time image. The experimental observation shows that it takes about 12 ns for the main streamer to penetrate the discharge gap and reach the cathode surface, and the average propagation velocity of the streamer is estimated to be about $5.83\times10^{5}$ m s$^{-1}$, which is consistent with that reported in the literature [58–60].

In fact, the electron density, electric field and space charge distribution inside the plasma are affected by the geometry of the streamer channel. In a fluidized-bed system, the streamer channel and the particle location have a lot of uncertainties. Hence, it is of great significance to study how the spatial position affects the streamer propagation. Three representative particle positions are selected to investigate streamer propagation, namely the tip of pin (position 1), the middle of discharge gap (position 2), and the cathode surface (position 3). Figures 5(b)–(d) show time-resolved ICCD images of streamer discharge evolution with fluidized particle placed in three different positions. When the fluidized particle is placed at position 1, the streamer discharge first initiates at the contact point between the pin electrode and the fluidized particle. It can be seen from figure 5(b) that a small discharge point appears at 27 ns near the pin electrode. This is caused by the polarization effect of the dielectric rod, resulting in an enhanced electric field at the contact point. The electrons in this region can absorb enough energy to initiate a discharge [24]. Subsequently, a surface streamer is formed and begins to propagate along the curved surface of the fluidized particle. This is because a large amount of space charges in the streamer will charge the surface of particles, and the electric field strength of the streamer head is rapidly amplified at the interface of the streamer and the fluidized particle, causing a strong electric field difference between the plasma, the solid surface and the neutral gas, thereby promoting the generation and propagation of surface discharges [61, 62]. When the streamer reaches the position with an angle of 31° from the equatorial plane of the fluidized particle, it leaves the fluidized particle surface and develops downward in a 'parabola-like' shape, reaching the cylinder surface at 48 ns. The entire streamer propagation process includes the following two discharge modes: volume discharge and surface discharge.

When the fluidized particle is located at position 2 (figure 5(c)), it can be seen from the discharge image that the initiation time of the streamer is delayed about 6 ns. After that, a streamer development process similar to figure 5(b) began to appear. When the fluidized particle is placed on the cathode surface (position 3), as shown in figure 5(d), the main streamer channel propagates approximately linearly before the streamer reaches the surface of the fluidized particle. After that, the streamer can propagate along the surface to near the equator, and then develop toward the cathode. This is due to the weak interaction between the plasma and the fluidized particle, causing the streamer away from the rod surface during propagation

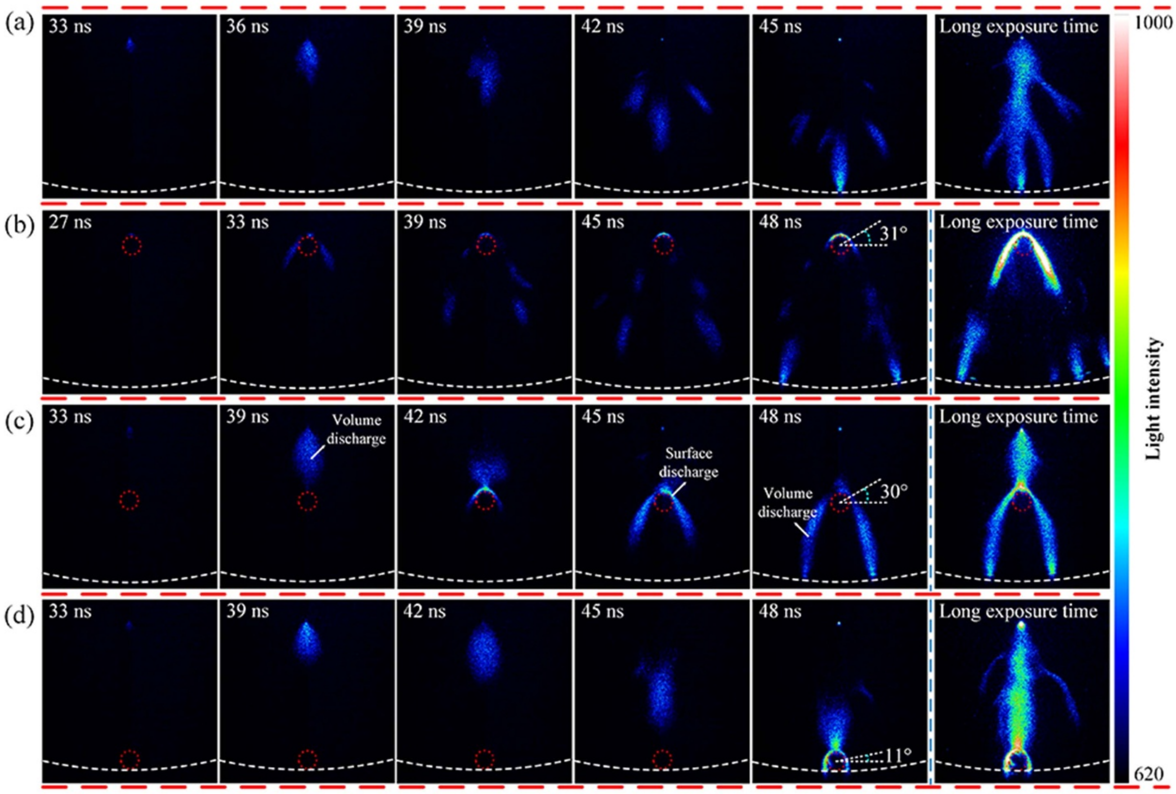


**Figure 5.** Time-resolved images of streamer propagation; (a) without fluidized particle, (b) position 1, (c) position 2, (d) position 3 with fluidized particle.

[17]. Comparing the fluidized particle in position 1 to position 3, the streamer covers a larger area on the surface of fluidized particle, which indicates that the plasma modification area increases, producing a better plasma modification effect. Compared with the non-fluidized particle, the presence of fluidized particle will cause the main streamer to split into two independent sub-streamers for propagation. The average propagation velocities of the streamer in the three positions are $3.53 \times 10^5$ m s$^{-1}$, $4.79 \times 10^5$ m s$^{-1}$ and $4.69 \times 10^5$ m s$^{-1}$, respectively, which are all smaller than that of without fluidized particle.

In order to better elucidate the plasma discharge behavior, a 2D numerical simulation model is used to calculate the time-resolved evolution of the electron density and electric field. The simulated 2D electron density distribution and electric field evolution without and with fluidized particle are demonstrated in figure 6. In the initial stage under both conditions, the electric field at the tip of the pin is higher (>600 Td) due to the small curvature radius, forming a corona discharge, which produces a large number of electrons and positive ions. The higher electric field of the streamer head can form an electronic avalanche, and the electrons will move to the pin electrode and distribute in the entire discharge channel. In the process of streamer propagation, the ionization processes are predominant. With the development and evolution of the main streamer, the streamer channel becomes wider and the head becomes brighter. When the streamer reaches the cathode surface, the electron density in the streamer channel with fluidized particle is $3.3 \times 10^{19}$ m$^{-3}$, which is lower than the electron density without fluidized particle ($1.4 \times 10^{20}$ m$^{-3}$). Indeed, the propagation of streamer discharge along the fluidized particle will be accompanied by the generation of high concentrations of active species, which plays a key role in plasma modification. The simulation results show that the maximum electron density generated by surface discharge is one order of magnitude higher than that produced by volume discharge, indicating that surface discharge plays a dominant role in powder modification. When the streamer arrives at the cathode surface, the electron densities of streamer head without and with fluidized particle reach $1.2 \times 10^{21}$ m$^{-3}$ and $2.5 \times 10^{20}$ m$^{-3}$, respectively.

When the streamer head develops towards the cathode, the electric field in this electric field region decreases rapidly (<100 Td), and the streamer channel is in a plasma state. At 60 ns, the streamer propagation distance is 1.7 mm in the absence of fluidized particle, and only 1.5 mm in the presence of fluidized particle, indicating that the existence of fluidized particle will hinder the streamer propagation. This is due to the polarization effect of fluidized particle in the electric field compared to non-fluidized particle. It can be observed that the electric field inside the particle is smaller than that of in gas phase, about 120 Td. Meanwhile, the electric field strength is enhanced at the upper and lower poles of the particle, reaching about 550 Td and 200 Td respectively at 65 ns, which is higher

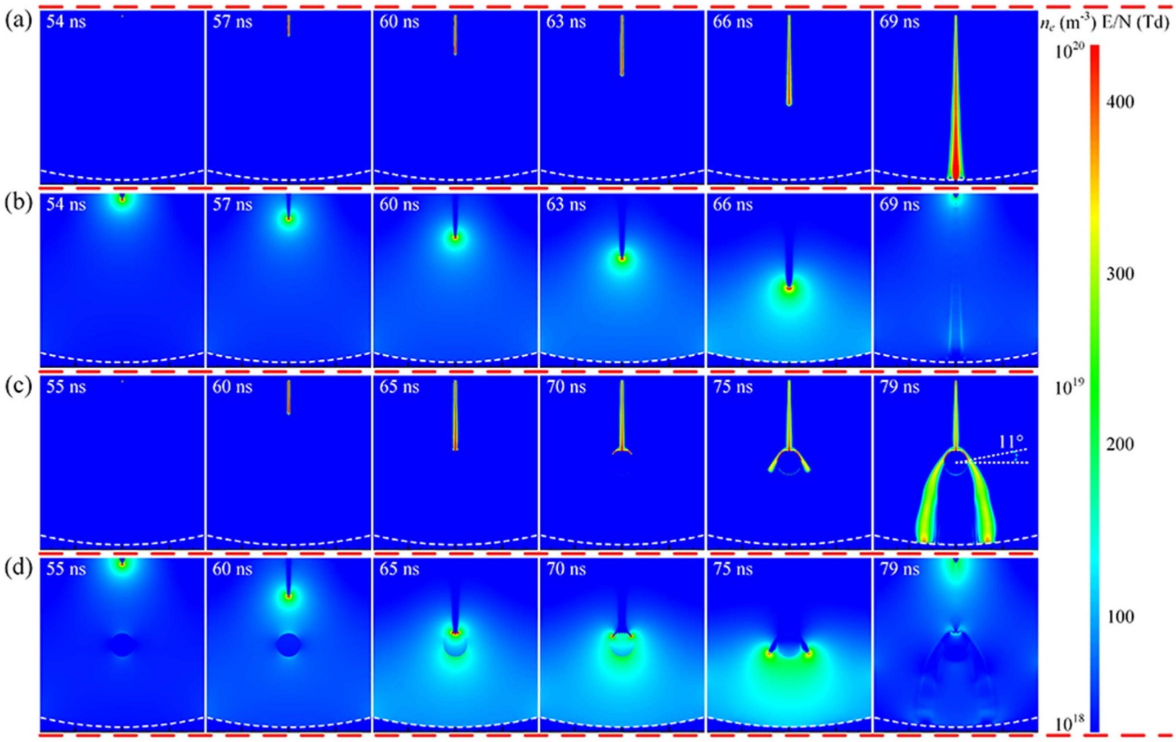


**Figure 6.** Simulated spatio-temporal distributions of the electron density (a) and electric field (b) without fluidized particle; the electron density (c) and electric field (d) with fluidized particle during streamer propagation.

than the gas phase electric field (140 Td), and the polarization electric field gradually increases with the streamer propagation. The electric field at the equator of the particle is the smallest, because the vector electric field generated here is perpendicular to the surface normal. Kong *et al* [6] investigated the interaction of plasma jet with a single fiber through a 2D fluid model. It is found that due to pre-ionization, the accumulation of positive charges at the south pole of the fiber would generate a repulsive force, hindering the propagation of positive charges in front of the ionization wave. In addition, the presence of fluidized particle reduces the average propagation velocity of the streamer. This is due to the fact that the fluidized particle distorts the streamer propagation path, which acts as a mechanical obstacle for streamer advancement in the gas phase, thus reducing the average streamer propagation velocity [63]. The closer to the cathode, the faster the streamer velocity. Parameters related to plasma modification that are not available through experiment can be obtained based on the numerical model, such as the distribution of active species on powder particles, which will be discussed in detail later.

### *3.2. Time-resolved evolution with multiple fluidized particles*

The ratio of gas to powder (gas-powder ratio) in the plasma fluidized-bed is an important operating parameter, which can significantly affect the fluidity, mixing and reactivity of the fluidized-bed. A low gas-powder ratio means that there is a higher concentration of powder particles, which may lead to particle accumulation and uneven distribution, hindering the mixing of gas and powder in the bed, and is not conducive to powder processing. Conversely, a high gas-powder ratio may cause excessive particle dispersion, resulting in unstable fluidization, and increase the drift and loss of particles in the bed.

Considering the complexities and randomness of particle behavior in plasma fluidized-bed systems, a typical case is selected for research. It assumes that the arrangement of particles is ordered. In the model, five particles are selected and arranged to cover two kinds of interactions between particles, namely direct interactions (between adjacent particles) and indirect interactions (between separated particles). Figures 7(a) and (b) show the streamer evolution with a distance 0.1 mm and 0.5 mm between adjacent fluidized particles in mode 1. Increasing the distance between adjacent fluidized particles has no effect on the plasma propagation path. The streamer first propagates in a straight line to the upper surface of the fluidized particle 1, and subsequent surface discharge formation is related to charge deposition, which creates an electrical component parallel to the surface [21]. As the distance between the adjacent particles increases from 0.1 mm to 0.5 mm, the area of the particles wrapped by the streamer increases. For example, for particle 5, as the distance increases from 0.1 mm to 0.5 mm, the particle area wrapped by the streamer is increased by 67%, indicating that plasma treatment of powder particles is more fully, facilitating a more extensive surface modification. Comparing the experimental (figure 7) and simulation results (figure 8), it was found that the streamer coverage area on the particle 1 surface is basically the same, approximately 43%, indicating good agreement of simulation and experiment results.

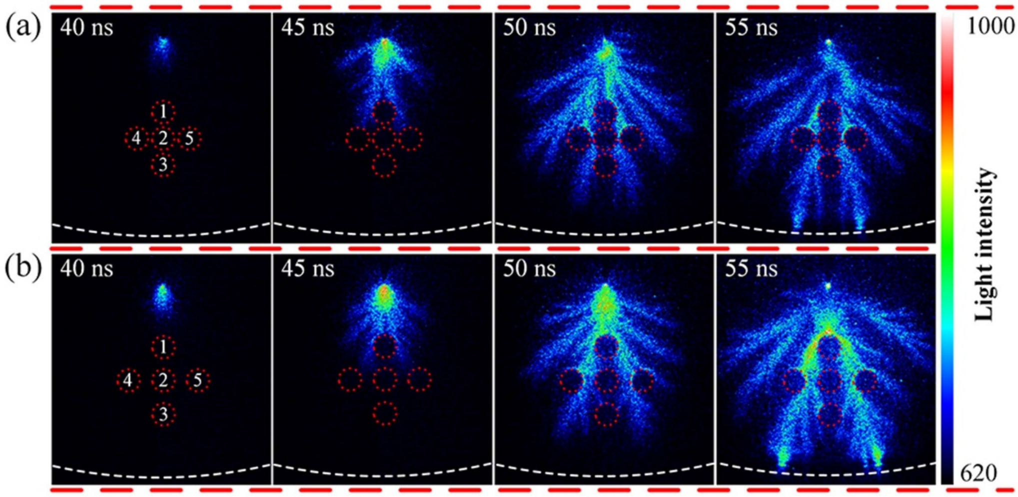


**Figure 7.** Streamer evolution with a distance of 0.1 mm (a) and 0.5 mm (b) between adjacent fluidized particles in mode 1.

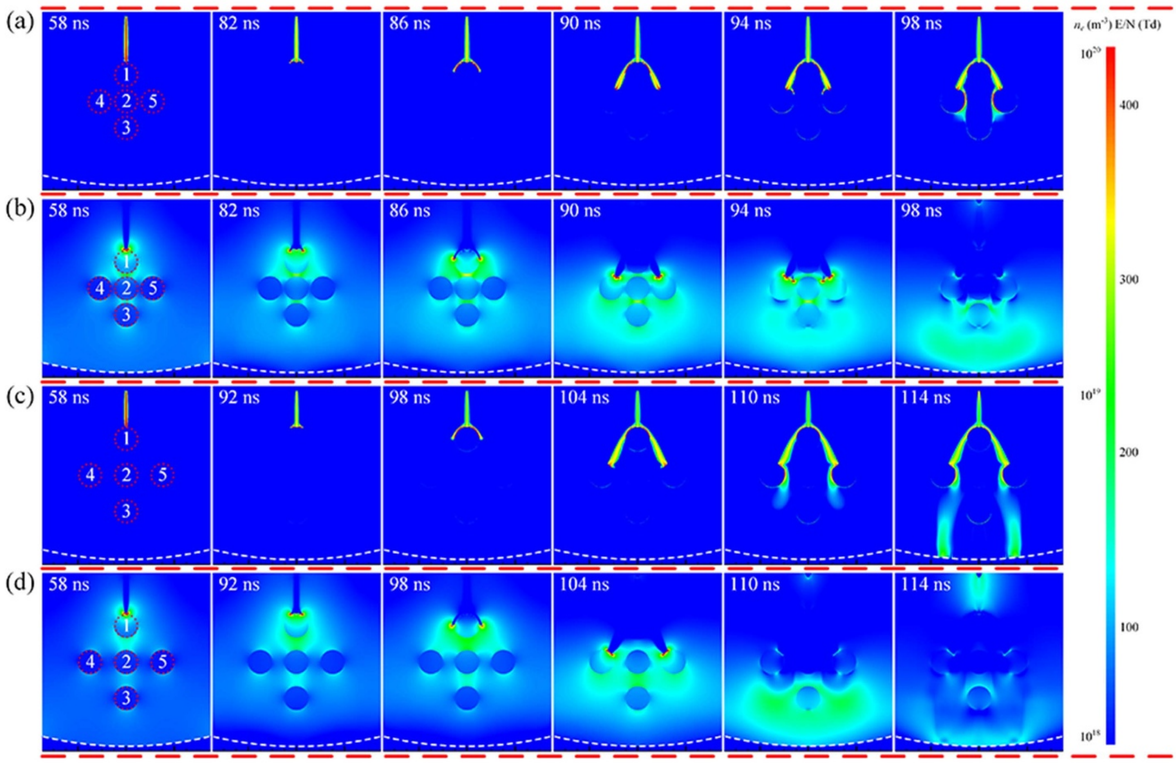


**Figure 8.** Simulation results: distribution of electron density (a), (c) and electric field (b), (d) with a distance 0.1 mm and 0.5 mm between adjacent fluidized particles in mode 1.

To better explore the streamer generation and propagation characteristics with multiple fluidized particles, the time-resolved evolution of the electron density and electric field are presented in figure 8. The plasma hits the surface of fluidized particle 1, and charged particles will charge the surface of particle 1. As the distance between adjacent particles increases, it can be seen that the development process of the entire streamer is longer, which is mainly due to the prolongation of the charging process on the surface of particle 1. The charge deposition will hinder the further development of the streamer discharge. When the adjacent distance is 0.1 mm (figure 8(a)), the streamer propagation is restricted between fluidized particles 2 and 5 due to the polarization between particles, and plasma cannot propagate further downward through the gap between fluidized particles 2 and 5 to form volume discharge as observed in the experiment.

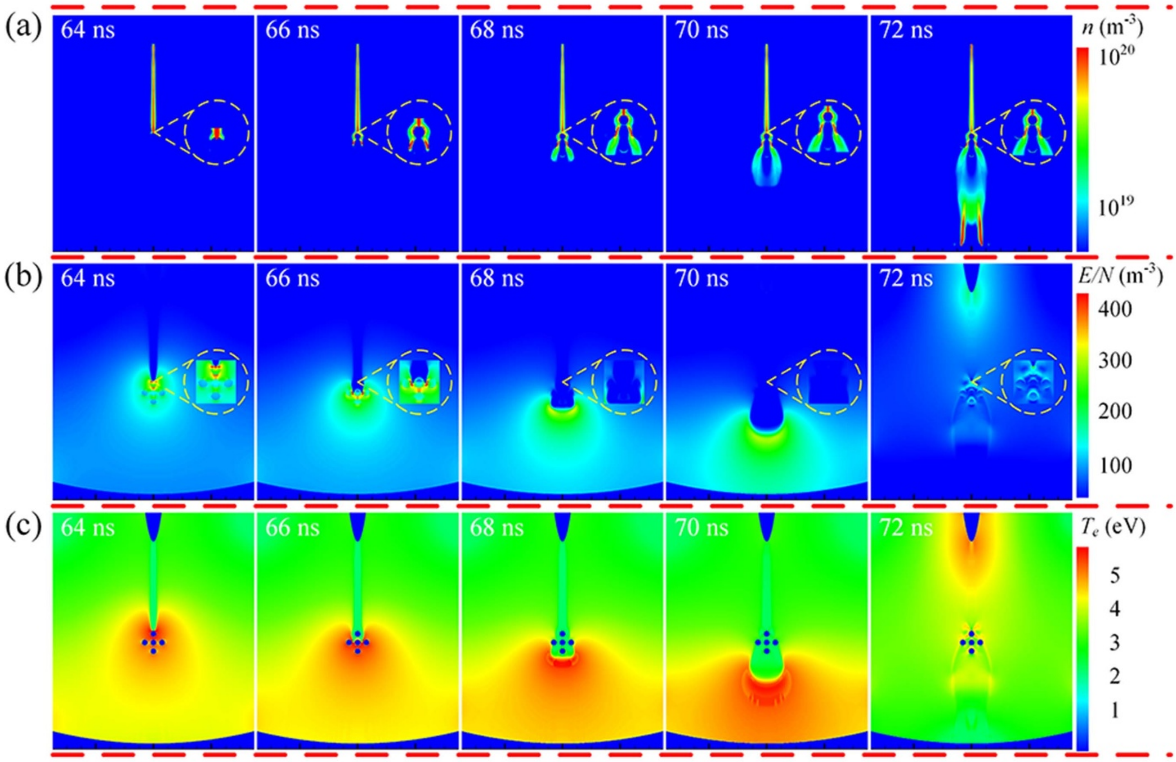


**Figure 9.** Simulated dynamics of electron density (a), electric field (b) and electron temperature (c) for micron-size particles (200 $\mu$m) in mode 1 (with the same number and mode as figure 8).

For example, the average velocities of streamer propagation on fluidized particle 1 and 5 is about $7.8 \times 10^4$ m s$^{-1}$ and $9.8 \times 10^4$ m s$^{-1}$, respectively. Both are lower than that of a single fluidized particle, which suggests that, for the geometries considered here, multiple fluidized particles can hinder streamer development. After the streamer reaches the particle surface (86 ns), the electron densities on the plasma channel and particle 1 surface are $3.2 \times 10^{19}$ m$^{-3}$ and $1.5 \times 10^{20}$ m$^{-3}$ respectively. The electron density on the surface of particle 5 is slightly increased to $1.9 \times 10^{20}$ m$^{-3}$. As the distance between adjacent particles increases from 0.1 mm to 0.5 mm (figure 8(c)), the repulsive coulomb force would decrease, and the streamer can propagate to the cathode surface, as observed in the experiment. However, compared with the distance of 0.1 mm, the electron densities of plasma channel, particle 1 and particle 5 surface all decrease to a certain extent. Comparing the experiment and simulation results, the streamer propagation path is basically the same, which indicates good qualitative agreement of theoretical and experimental results.

As mentioned above, the fluidized particles in the electric field will cause internal charge polarization, and the local electric field inside and near the adjacent fluidized particles will also affect plasma propagation. To further study the local electric field distribution between the fluidized particles, figures 8(b) and (d) show the time-resolved evolution of the corresponding electric field strength distribution. During streamer evolution, the streamer head is always in the high electric field region, and the electric field strength behind the streamer head decreases rapidly. That is because the charges in the streamer neutralize the opposite charge on the particles surface [20]. As the distance increases from 0.1 mm to 0.5 mm, the electric field at the streamer head will decrease from 550 Td to 430 Td, and the polarization electric field between the upper and lower poles of the particles will also weaken. For example, at 86 ns, the polarized electric fields of the upper and lower poles of particle 2 are 330 Td and 200 Td, 240 Td and 150 Td, respectively, and the electric fields near the equator are only 100 Td and 75 Td. Moreover, as the streamer develops, the polarization phenomenon becomes more and more obvious, which can be also observed in the vicinity of fluidized particles 2 and 3 and in the region where streamer reaches on the upper part of fluidized particle 5. However, the polarization of the fluidized particle did not further generate local micro-discharge.

It is a great challenge to operate and observe streamer evolution process for small-size fluidized particles (tens or hundreds of microns) compared to large-size fluidized particles (a few millimeters). Numerical simulation, as an alternative approach, can reduce the complexity of the experiment and provide a more flexible research platform, facilitating a comprehensive understanding of the fundamental physical processes of plasma and micron particles. Figure 9 demonstrates the dynamic behavior of the plasma and micron fluidized particles (200 $\mu$m) in mode 1. The streamer evolution process is consistent with that of the large fluidized particles (1000 $\mu$m), but the average streamer propagation velocity is faster. It can be seen from the figure that as the particle size decreases from 1000 $\mu$m to 200 $\mu$m, the area of particle 1 covered by the streamer is increased by 78%, indicating that the smaller size of particle is favorable to the plasma surface treatment of powder particles. It is worth noting that the polarization between the upper and lower poles of the fluidized particle 1 is significantly enhanced, reaching 750 Td and 400 Td respectively. Moreover, an interesting phenomenon in the evolution of the electric field is that when the streamer passes through the gap between fluidized particles 2 and 5, the high-field regions of the two streamer heads merge and advance towards the cathode. The two streamers do not propagate separately as before, but the electric field at this time is significantly reduced compared with the fluidized particle, which is only 300 Td. Figure 9(c) shows the evolution of electron temperature. Due to the strong electric field and the high ionization at the streamer head, the electron temperature is large, i.e. above 5 eV followed by a quasi-neutral conductive channel, and the electron temperature in the channel is about 0.5 eV. Once the conductive channel is established (72 ns), the electron temperature gradually decreases to about 2 eV. The evolution of electron temperature is consistent with that of electric field.

### *3.3. Distribution of reactive species on the fluidized particle surface*

The highly chemical reactive species generated in plasma channel can play a leading role in the plasma modification or powder treatment processes. Therefore, it is crucial to study the production and spatial distribution behavior of reactive species during the streamer propagation to gain a deeper understanding of plasma modification. Figure 10 shows a schematic diagram of the right hemisphere of the fluidized particle (0° to 180°). Notably, the streamer propagation time on the particles surface for two various fluidized particle sizes are different. For the particle size of 200 $\mu$m, the streamer development time is only 2 ns, and the corresponding density profile of the evolution is taken between 64 ns and 65 ns. Nevertheless, the streamer development time on the particle surface lasts for 9 ns for a particle size of 1000 $\mu$m, and thus the density profile of the evolution is taken between 78 ns and 87 ns.

Evolution of the excited species (N and O) and ions ($N_2^+$ and $O_2^-$) on the surface of 200 $\mu$m (left) and 1000 $\mu$m (right) fluidized particles 1 in mode 1 are presented in figure 11. For the particle size of 200 $\mu$m, the maxima of the number densities of N, O and $O_2^-$ all appear at the north pole, and the

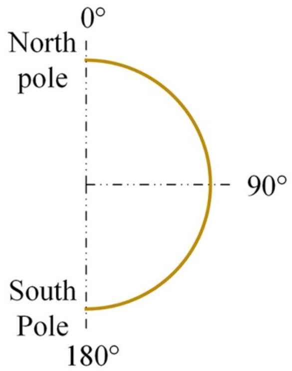


**Figure 10.** Schematic diagram of the right hemisphere of the fluidized particle (0° to 180°).

corresponding minima of the number densities are obtained at the south pole. The maximum values reach $6.1 \times 10^{18}$ m$^{-3}$, $3.3 \times 10^{21}$ m$^{-3}$ and $5.1 \times 10^{18}$ m$^{-3}$ at 0°, respectively, and the minimum values appear at 180°, which are $3.2 \times 10^{13}$ m$^{-3}$, $1.9 \times 10^{19}$ m$^{-3}$ and $2.0 \times 10^{16}$ m$^{-3}$, respectively. The maximum of the number density of $N_2^+$ is obtained at 35° with $4.3 \times 10^{18}$ m$^{-3}$, and the minimum is obtained at 180° with $5.8 \times 10^{16}$ m$^{-3}$. For the particle size of 1000 $\mu$m, the number densities of O and $O_2^-$ first decrease and then slightly increase from 0° to 180°. After that, the number densities gradually decrease. The number densities of O and $O_2^-$ achieve a maximum of $2.8 \times 10^{21}$ m$^{-3}$ and $3.9 \times 10^{18}$ m$^{-3}$ at the north pole of the particle, respectively. The N number density decreases sharply and also reaches a maximum value of $1.0 \times 10^{18}$ m$^{-3}$ at the north pole. The maxima of the number density of $N_2^+$ is obtained at 50° with $7.5 \times 10^{17}$ m$^{-3}$. The minima of N, O, $N_2^+$ and $O_2^-$ number densities are obtained at the south pole with $2.0 \times 10^{7}$ m$^{-3}$, $4.3 \times 10^{16}$ m$^{-3}$, $7.7 \times 10^{13}$ m$^{-3}$ and $1.0 \times 10^{12}$ m$^{-3}$, respectively. As the particle size decreases, the maximum number densities of all active particles increase.

When the streamer reaches the particle surface, the surface charges begin to accumulate, initiating a charging process, so the number of active species at the north pole is denser. As the surface discharge propagates, the collision between ions and the particle surface will induce emission of secondary electrons, which forms a thin sheath of about tens of microns in thickness between the streamer head and the particle boundary. In this sheath, the electron density is relatively low, resulting in a decrease in the number density of active species. As mentioned above, the streamer coverage area increases as the particle size decreases from 1000 $\mu$m to 200 $\mu$m. The position of streamer away from the surface of 200 $\mu$m particle is about 160°, which is higher than that of the 1000 $\mu$m particle. Therefore, the number densities of active species with a particle size of 200 $\mu$m after 90° is higher.

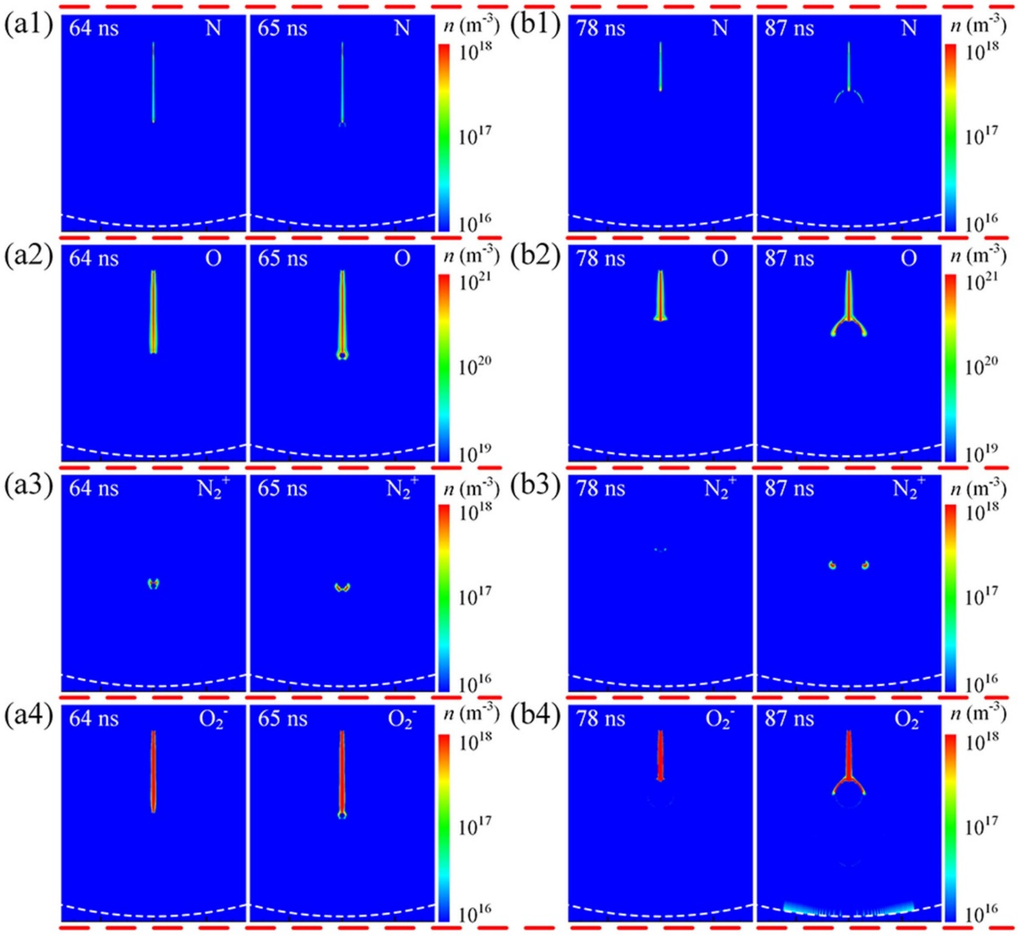


**Figure 11.** Evolution of the reactive species on the surface of 200 $\mu$m (left) and 1000 $\mu$m (right) fluidized particles 1 in mode 1.

## 4. Conclusion

In this work, the time-resolved evolution behavior of streamer on the fluidized particles surface is investigated in a simplified pin-cylinder configuration plasma fluidized-bed system under different fluidization conditions. The main conclusions are drawn as follows:

(1) The presence of fluidized particle will cause streamer branching, and the main streamer splits into two independent sub-streamers for propagation in a 'parabola-like' shape, and the streamer average propagation velocity decreases. For multiple fluidized particles, compared with large-size fluidized particles (1000 $\mu$m), streamer will gradually wrap micron-size fluidized particles (200 $\mu$m), and the area of particle wrapped by the streamer is increased by 78%, which is favorable to the modification of powder particles. The entire streamer propagation process includes volume discharge and surface discharge. The simulation results show that the maximum electron density generated by surface discharge is one order of magnitude higher than that produced by volume discharge, which indicates that surface discharge plays a dominant role in powder modification.

(2) In the field of plasma modification, active species play a leading role. The evolution of reactive species on the particle surface during streamer propagation is analyzed. The active species (N, O, $O_2^-$) are mainly distributed around the north pole, and $N_2^+$ is mainly distributed between 25° and 50° of the particles. With the decrease of fluidized particle size, the maxima of the number densities of active species increase.

In summary, this work provides valuable insights into the dynamic behavior of streamer discharge on fluidized particles through experiment and numerical simulation, and contributes to a deeper understanding of plasma fluidized-bed powder treatment.

## Data availability statement

All data that support the findings of this study are included within the article (and any supplementary files).

## Acknowledgments

This work is supported by the National Natural Science Foundation of China (Grant Nos. 52177130 and 52377137).

## ORCID iDs

Ju Li https://orcid.org/0000-0001-6616-8330
Nan Jiang https://orcid.org/0000-0003-4938-5864
Xiaolong Wang https://orcid.org/0000-0002-6229-2470
Guanglin Yu https://orcid.org/0000-0002-4753-6414
Bangfa Peng https://orcid.org/0000-0002-8690-0872
Junwen He https://orcid.org/0009-0002-9462-0077
Jie Li https://orcid.org/0000-0001-5557-8721

## References

[1] Li J, Yao S, Xiao F and Amirkhanian S N 2022 Surface modification of ground tire rubber particles by cold plasma to improve compatibility in rubberised asphalt *Int. J. Pavement Eng.* **23** 651–62
[2] Kusano Y 2014 Atmospheric pressure plasma processing for polymer adhesion: a review *J. Adhes.* **90** 755–77
[3] Wang R, Xia Z, Kong X, Xue S and Wang H 2022 Uniform deposition of silicon oxide film on cylindrical substrate by radially arranged plasma jet array *Surf. Coat. Technol.* **437** 128365
[4] Booth J-P, Mozetič M, Nikiforov A and Oehr C 2022 Foundations of plasma surface functionalization of polymers for industrial and biological applications *Plasma Sources Sci. Technol.* **31** 103001
[5] Samanta K K, Joshi A G, Jassal M and Agrawal A K 2021 Hydrophobic functionalization of cellulosic substrate by tetrafluoroethane dielectric barrier discharge plasma at atmospheric pressure *Carbohydrate Polym.* **253** 117272
[6] Kong X, Xue S, Li H, Yang W, Martynovich E, Ning W and Wang R 2022 Simulation study on an atmospheric pressure plasma jet interacting with a single fiber: effects of the fiber's permittivity *Plasma Sources Sci. Technol.* **31** 095010
[7] Liu K, Xia H, Yang M, Geng W, Zuo J and Ostrikov K K 2022 Insights into generation of OH radicals in plasma jets with constant power: the effects of driving voltage and frequency *Vacuum* **198** 110901
[8] Liu K, Duan Q, Zheng Z, Zhou R, Zhou R, Tang W, Cullen P and Ostrikov K 2021 Gas-phase peroxynitrite generation using dielectric barrier discharge at atmospheric pressure: a prospective sterilizer *Plasma Process. Polym.* **18** 2100016
[9] Yao S, Ma Y, Xu T, Wang Z, Lv P, Zheng J, Ma C, Yu K, Wei W and Ostrikov K K 2021 Ti–C bonds reinforced $TiO_2$@ C nanocomposite Na-ion battery electrodes by fluidized-bed plasma-enhanced chemical vapor deposition *Carbon* **171** 524–31
[10] Snyder H R, Currier R P and Murillo M S 2000 Plasma fluidized bed imaging and possible strong coupling effects *Appl. Phys. Lett.* **76** 2511–3
[11] Derco J, Lodes A, Lapcik L and Blecha J 1984 Application of plasmochemical processes in treatment of properties of macromolecular materials. II. Surface treatment of polypropylene by oxygen-nitrogen plasma in the fluidized bed *Chem. Pap.* **38** 463–70
[12] Chen G, Chen S, Zhou M, Feng W, Gu W and Yang S 2006 Application of a novel atmospheric pressure plasma fluidized bed in the powder surface modification *J. Phys. D: Appl. Phys.* **39** 5211–5
[13] Soto G, Tiznado H, Contreras O, Pérez-Tijerina E, Cruz-Reyes J, Del Valle M and Portillo A 2011 Preparation of a Ag/$SiO_2$ nanocomposite using a fluidized bed microwave plasma reactor, and its hydrodesulphurization and Escherichia coli bactericidal activities *Powder Technol.* **213** 55–62
[14] Bouchoul N, Touati H, Fourre E, Clacens J-M and Batiot-Dupeyrat C 2021 Efficient plasma-catalysis coupling for $CH_4$ and $CO_2$ transformation in a fluidized bed reactor: comparison with a fixed bed reactor *Fuel* **288** 119575
[15] Dasan B G, Boyaci I H and Mutlu M 2017 Nonthermal plasma treatment of Aspergillus spp. spores on hazelnuts in an atmospheric pressure fluidized bed plasma system: impact of process parameters and surveillance of the residual viability of spores *J. Food Eng.* **196** 139–49
[16] Jiang N, Qu Y, Zhu J, Wang H, Li J, Shu Y, Cui Y, Tan Y, Peng B and Li J 2023 Remediation of atrazine-contaminated soil in a fluidized-bed DBD plasma reactor *Chem. Eng. J.* **464** 142467
[17] Li Y, Yang D-Z, Qiao J-J, Zhang L, Wang W-Z, Zhao Z-L, Zhou X-F, Yuan H and Wang W-C 2020 The dynamic evolution and interaction with dielectric material of the discharge in packed bed reactor *Plasma Sources Sci. Technol.* **29** 055004
[18] Kim H-H, Teramoto Y and Ogata A 2016 Time-resolved imaging of positive pulsed corona-induced surface streamers on $TiO_2$ and $\gamma$-$Al_2O_3$-supported Ag catalysts *J. Phys. D: Appl. Phys.* **49** 415204
[19] Korolev I, Liu Y, Mussenbrock T and Schulze J 2022 Propagation dynamics and interaction of multiple streamers at and above adjacent dielectric pellets in a packed bed plasma reactor *J. Phys. D: Appl. Phys.* **55** 495201
[20] Xiong R, Zhao P, Wang H, Zhang Y and Jiang W 2020 Impact of different packing beads methods for streamer generation and propagation in packed-bed dielectric barrier discharge *J. Phys. D: Appl. Phys.* **53** 185202
[21] Engeling K W, Kruszelnicki J, Kushner M J and Foster J E 2018 Time-resolved evolution of micro-discharges, surface ionization waves and plasma propagation in a two-dimensional packed bed reactor *Plasma Sources Sci. Technol.* **27** 085002
[22] Cheng H, Ma M, Zhang Y, Liu D and Lu X 2020 The plasma enhanced surface reactions in a packed bed dielectric barrier discharge reactor *J. Phys. D: Appl. Phys.* **53** 144001
[23] Kang W S, Kim H-H, Teramoto Y, Ogata A, Lee J Y, Kim D-W, Hur M and Song Y-H 2018 Surface streamer propagations on an alumina bead: experimental observation and numerical modeling *Plasma Sources Sci. Technol.* **27** 015018
[24] Van Laer K and Bogaerts A 2015 Fluid modelling of a packed bed dielectric barrier discharge plasma reactor *Plasma Sources Sci. Technol.* **25** 015002
[25] Van Laer K and Bogaerts A 2017 Influence of gap size and dielectric constant of the packing material on the plasma behaviour in a packed bed DBD reactor: a fluid modelling study *Plasma Process. Polym.* **14** 1600129
[26] Van Laer K and Bogaerts A 2017 How bead size and dielectric constant affect the plasma behaviour in a packed bed plasma reactor: a modelling study *Plasma Sources Sci. Technol.* **26** 085007
[27] Wang W, Butterworth T and Bogaerts A 2021 Plasma propagation in a single bead DBD reactor at different dielectric constants: insights from fluid modelling *J. Phys. D: Appl. Phys.* **54** 214004
[28] Wang W, Kim H-H, Van Laer K and Bogaerts A 2018 Streamer propagation in a packed bed plasma reactor for plasma catalysis applications *Chem. Eng. J.* **334** 2467–79

[29] Kruszelnicki J, Engeling K W, Foster J E, Xiong Z and Kushner M J 2016 Propagation of negative electrical discharges through 2-dimensional packed bed reactors *J. Phys. D: Appl. Phys.* **50** 025203
[30] Zhu Y, Wu Y, Wei B, Xu H, Liang H, Jia M, Song H and Li Y 2020 Nanosecond-pulsed dielectric barrier discharge-based plasma-assisted anti-icing: modeling and mechanism analysis *J. Phys. D: Appl. Phys.* **53** 145205
[31] Chen X, Zhu Y, Wu Y, Hao J, Ma X and Lu P 2021 Numerical investigations of nanosecond surface streamers at elevated pressure *Plasma Sources Sci. Technol.* **30** 075008
[32] Zhu Y and Starikovskaia S 2018 Fast gas heating of nanosecond pulsed surface dielectric barrier discharge: spatial distribution and fractional contribution from kinetics *Plasma Sources Sci. Technol.* **27** 124007
[33] Zhu Y, Shcherbanev S, Baron B and Starikovskaia S 2017 Nanosecond surface dielectric barrier discharge in atmospheric pressure air: i. measurements and 2D modeling of morphology, propagation and hydrodynamic perturbations *Plasma Sources Sci. Technol.* **26** 125004
[34] Li M, Chen S, Zhu Y, Li Y, Wang F, Cui Y and Zhuang C 2023 Experimental and numerical investigation of surface streamers in a nanosecond pulsed packed bed reactor *Plasma Sources Sci. Technol.* **32** 064002
[35] Yu G, Jiang N, Peng B, Sun H, Liu Z and Li J 2023 Study on the plasma characteristics in a needle-plate dielectric barrier discharge with a rotating dielectric plate *J. Appl. Phys.* **133** 083302
[36] Chen X, Zhu Y and Wu Y 2020 Modeling of streamer-to-spark transitions in the first pulse and the post discharge stage *Plasma Sources Sci. Technol.* **29** 095006
[37] Zhu Y, Chen X, Wu Y, Hao J, Ma X, Lu P and Tardiveau P 2021 Simulation of ionization-wave discharges: a direct comparison between the fluid model and E-FISH measurements *Plasma Sources Sci. Technol.* **30** 075025
[38] Guo Y, Li Y, Zhu Y and Sun A 2023 A numerical and experimental study on positive diffusive ionization waves in different $N_2/O_2$ mixtures: the role of photoionization *Plasma Sources Sci. Technol.* **32** 025003
[39] Jiang Y, Wang Y, Zhang J and Wang D 2022 Numerical study of singlet delta oxygen ($O_2$ ($a^1\Delta_g$)) generation and transport in the $He/O_2$ atmospheric pressure plasma jet *J. Phys. D: Appl. Phys.* **55** 335203
[40] Volynets A V, Lopaev D, Rakhimova T, Proshina O, Chukalovsky A and Booth J-P 2020 Fast quenching of metastable $O_2$ ($a^1\Delta_g$) and $O_2$ ($b^1\Sigma_g{}^+$) molecules by O (3P) atoms at high temperature *Plasma Sources Sci. Technol.* **29** 115020
[41] Hoskinson A R, Rawlins W T, Galbally-Kinney K L, Gong E and Hopwood J 2021 Production and loss of $O_2$ ($^1\Delta_g$) at atmospheric pressure using microwave-driven microplasmas *J. Phys. D: Appl. Phys.* **55** 125208
[42] Bourdon A, Pasko V, Liu N Y, Célestin S, Ségur P and Marode E 2007 Efficient models for photoionization produced by non-thermal gas discharges in air based on radiative transfer and the Helmholtz equations *Plasma Sources Sci. Technol.* **16** 656–78
[43] Luque A, Ebert U, Montijn C and Hundsdorfer W 2007 Photoionization in negative streamers: fast computations and two propagation modes *Appl. Phys. Lett.* **90** 081501
[44] Itikawa Y 2006 Cross sections for electron collisions with nitrogen molecules *J. Phys. Chem. Ref. Data* **35** 31–53
[45] Itikawa Y 2009 Cross sections for electron collisions with oxygen molecules *J. Phys. Chem. Ref. Data* **38** 1–20
[46] Ionin A, Kochetov I, Napartovich A and Yuryshev N 2007 Physics and engineering of singlet delta oxygen production in low-temperature plasma *J. Phys. D: Appl. Phys.* **40** R25
[47] Capitelli M, Ferreira C M, Gordiets B F and Osipov A I 2013 *Plasma Kinetics in Atmospheric Gases* vol 31 (Springer)
[48] Kossyi I, Kostinsky A Y, Matveyev A and Silakov V 1992 Kinetic scheme of the non-equilibrium discharge in nitrogen-oxygen mixtures *Plasma Sources Sci. Technol.* **1** 207–20
[49] Guerra V and Loureiro J 1997 Self-consistent electron and heavy-particle kinetics in a low-pressure-glow discharge *Plasma Sources Sci. Technol.* **6** 373–85
[50] Zhang P and Kortshagen U 2005 Two-dimensional numerical study of atmospheric pressure glows in helium with impurities *J. Phys. D: Appl. Phys.* **39** 153–63
[51] Matzing H 1991 Chemical kinetics of flue gas cleaning by irradiation with electrons *Adv. Chem. Phys.* **80** 315–402
[52] Poggie J, Adamovich I, Bisek N and Nishihara M 2012 Numerical simulation of nanosecond-pulse electrical discharges *Plasma Sources Sci. Technol.* **22** 015001
[53] Peng B, Jiang N, Yao X, Ruan Y, Wang D, Shang K, Lu N, Namihira T, Li J and Wu Y 2019 Experimental and numerical studies of primary and secondary streamers in a pulsed surface dielectric barrier discharge *J. Phys. D: Appl. Phys.* **52** 325202
[54] Murakami T, Niemi K, Gans T, O'Connell D and Graham W G 2012 Chemical kinetics and reactive species in atmospheric pressure helium–oxygen plasmas with humid-air impurities *Plasma Sources Sci. Technol.* **22** 015003
[55] Inada Y, Aono K, Ono R, Kumada A, Hidaka K and Maeyama M 2017 Two-dimensional electron density measurement of pulsed positive primary streamer discharge in atmospheric-pressure air *J. Phys. D: Appl. Phys.* **50** 174005
[56] Ono R and Oda T 2003 Formation and structure of primary and secondary streamers in positive pulsed corona discharge—effect of oxygen concentration and applied voltage *J. Phys. D: Appl. Phys.* **36** 1952–8
[57] Nijdam S, Van De Wetering F, Blanc R, Van Veldhuizen E and Ebert U 2010 Probing photo-ionization: experiments on positive streamers in pure gases and mixtures *J. Phys. D: Appl. Phys.* **43** 145204
[58] Li Y, Van Veldhuizen E M, Zhang G-J, Ebert U and Nijdam S 2018 Positive double-pulse streamers: how pulse-to-pulse delay influences initiation and propagation of subsequent discharges *Plasma Sources Sci. Technol.* **27** 125003
[59] Inada Y, Komuro A, Ono R, Kumada A, Hidaka K and Maeyama M 2019 Two-dimensional electron density measurement of pulsed positive secondary streamer discharge in atmospheric-pressure air *J. Phys. D: Appl. Phys.* **52** 185204
[60] Eichwald O, Ducasse O, Dubois D, Abahazem A, Merbahi N, Benhenni M and Yousfi M 2008 Experimental analysis and modelling of positive streamer in air: towards an estimation of O and N radical production *J. Phys. D: Appl. Phys.* **41** 234002
[61] Min Z, Shengyu H, Zhang Y, Shuqun W and Zhang C 2022 Plasma propagation in single-particle packed dielectric barrier discharges: joint effects of particle shape and discharge gap *Plasma Sci. Technol.* **24** 065401
[62] Zhu M, Hu S, Wu F, Ma H, Xie S and Zhang C 2022 $CO_2$ dissociation in a packed bed DBD reactor: effect of streamer discharge *J. Phys. D: Appl. Phys.* **55** 225207
[63] Singh S and Serdyuk Y V 2018 Simulations of nonthermal electrical discharges in air over solid insulating barrier *IEEE Trans. Plasma Sci.* **47** 729–35